Advanced Review

GW method and Bethe–Salpeter equation for calculating electronic excitations

Xia Leng, Fan Jin, Min Wei and Yuchen Ma*

The introduction of GW approximation to the electron's self-energy by Hedin in the 1960s, where G and W denote the one-particle Green's function and the screened Coulomb interaction, respectively, facilitates the computation of quasiparticle energies through Dyson's equation. GW method can also help us determine the electron–hole interaction, which is a functional derivative of self-energy with respect to one-particle Green's function, with excellent accuracy, and its combination with Bethe–Salpeter equation, which is derived from two-particle Green's function, is a powerful tool to study electronic excitations and optical absorption. Thanks to the development of methodology and softwares during the last 30 years, the capability of GW method and Bethe–Salpeter equation to deal with real systems is elevated substantially, while they also exhibit many advantages over other first-principles methods in band structures, ionization potentials, electron affinities, optical spectra, and so on. They have been successfully applied in the excited states of various systems, including crystals, metals, nanomaterials, chemical and biological systems, and so on.

How to cite this article:
WIREs Comput Mol Sci 2016, 6:532–550. doi: 10.1002/wcms.1265

INTRODUCTION

In 1948, Feynman defined a propagation function,[1] which is usually called one-particle Green's function later, to describe the motion of a free particle in space and time in the quantum field theory. Three years later, Schwinger defined the two-particle Green's function.[2] After then, Green's function technique is extensively adopted in many-body physics, nuclear physics, statistical mechanics, and so on. The topic that will be presented in this review is its applications in excited states of real systems that are interested in material science, chemistry and biology.

Excited states discussed here comprise charged excitations, where the number of electrons in the system changes from N to $N - 1$ or $N + 1$, and neutral excitations, where the number of electrons remains constant. In the $|N\rangle \rightarrow |N - 1\rangle$ case, an electron in the valence band (occupied orbital) is kicked out the system by photon irradiation. In the $|N\rangle \rightarrow |N + 1\rangle$ case, an electron from infinity falls into the conduction band (unoccupied orbital), emitting a photon simultaneously. These two processes are related to the photoemission spectroscopy and inverse photoemission spectroscopy, respectively, through which we can study the electronic structure, ionization potential, and electron affinity of materials and molecules. In the $|N\rangle \rightarrow |N\rangle$ case, an electron in the valence band is boosted into the conduction band after absorbing a photon, leaving a hole in the valence band. The excited electron and the hole left behind are coupled together by Coulomb interaction, forming an exciton. The energy and oscillator strength of the exciton can be measured through optical absorption spectroscopy. The electronic structure, exciton energy, and the corresponding wave functions can be determined from one- and two-particle Green's

*Correspondence to: myc@sdu.edu.cn

School of Chemistry and Chemical Engineering, Shandong University, Jinan, China

Conflict of interest: The authors have declared no conflicts of interest for this article.

functions as these physical quantities appear in the formalisms of Green's functions in the energy space. For example, the electron addition and removal energies are the poles of one-particle Green's function.[3] Green's function technique is an alternative approach to the more common first-principles approaches such as density-functional theory (DFT), time-dependent DFT, and wave function-based ones including coupled-cluster theory, complete active space self-consistent field theory, quantum Monte Carlo theory, and so forth, to interpret experimental spectra.

Green's function method has been developed in different ways by the communities of quantum chemistry and condensed-matter physics. Early attempts toward using Green's functions in quantum chemistry started from the late 1960s. Till now, techniques including outer-valence Green's function approximation and second- or third-order algebraic diagrammatic construction method have been introduced. Detailed information on this respect can be referred to in a recent review by Danovich.[4] In this review, we will discuss an alternative Green's function technique, GW method and its combination with Bethe–Salpeter equation (BSE), which has been well known in the condensed-matter physics community for excited states calculation. The key ingredient of Green's function method is the electron's self-energy Σ, which embodies the complicated many-body exchange and correlation interactions among particles. In 1965, Hedin introduced a closed set of four integro-differential equations which connect self-energy, screened Coulomb potential (W), irreducible polarizability (P), and vertex function (Γ).[5] These equations, together with Dyson's equation which describes the motion of one-particle Green's function,[6] form a set of coupled equations from which the exact one-particle Green's function and self-energy can be determined in principle through a self-consistent scheme as proposed by Hedin.[5] This is not an easy task, so Hedin invented the famous GW method, i.e., the self-energy is computed approximately via $\Sigma = iGW$ where G is the one-particle Green's function.[5] Applying it to the quasiparticle (QP) equation which is the transformation of the Dyson's equation under QP approximation, we could get electronic structures that are in excellent agreement with photoemission and inverse photoemission spectroscopies. The application of GW method in real materials boomed after the pioneering work by Hybertsen and Louie in 1985.[7] GW method greatly remedied the failure of local-density approximation (LDA) in DFT in band gap calculations for semiconductors at that time. Although some hybrid exchange-correlation functionals have been developed in order to improve the accuracy of DFT for band gap prediction, empirical parameters still imbedded in these functionals may limit their transferability.

In 1951, Salpeter and Bethe derived the motion equation for two-particle Green's function, i.e., BSE.[8] Sham et al. extended it to the exciton case in the mid of 1960s and studied the optical absorption spectra of bulk diamond and silicon using model functions to describe electron–hole interactions.[9–11] In 1961, Baym and Kadanoff proposed an exact formula $K = \delta\Sigma/\delta G$ to compute the electron–hole interaction (K), i.e., K is a functional derivative of self-energy with respect to one-particle Green's function.[12] In 1982, Strinati introduced a scheme that makes first-principles calculations of excitons feasible based on BSE, GW method, and the Baym–Kadanoff theory.[13] The full first-principles calculation of excitons was realized by Onida et al. in 1995 on a Na_4 cluster according to Strinati's scheme.[14] With the development of methodology and *ab initio* software package in GW method and BSE together with the increasing computer power, the usage of GW method and BSE expands enormously in recent years as can be seen from the increase of related literatures. There have been several reviews on GW method and BSE.[3,15–22] Here, we only briefly present some of the main points of GW method and BSE, some methodology development and various applications in recent years.

ONE-PARTICLE GREEN'S FUNCTION

One-particle Green's function describes the electron addition or removal process in the system. If $|N, 0\rangle$ stands for the ground state of the N-electron system, the one-particle Green's function is defined as

$$\begin{aligned} G(\mathbf{r}_1 t_1, \mathbf{r}_2 t_2) &= -i\langle N,0|T\left[\hat{\psi}(\mathbf{r}_1 t_1)\hat{\psi}^{\dagger}(\mathbf{r}_2 t_2)\right]|N,0\rangle \\ &= \begin{cases} -i\langle N,0|\hat{\psi}(\mathbf{r}_1 t_1)\hat{\psi}^{\dagger}(\mathbf{r}_2 t_2)|N,0\rangle & if \quad t_1 > t_2 \\ i\langle N,0|\hat{\psi}^{\dagger}(\mathbf{r}_2 t_2)\hat{\psi}(\mathbf{r}_1 t_1)|N,0\rangle & if \quad t_2 > t_1 \end{cases} \end{aligned} \tag{1}$$

where $\hat{\psi}^{\dagger}(\mathbf{r}t)$ and $\hat{\psi}(\mathbf{r}t)$ are the fermion creation and annihilation operators in the Heisenberg representation, respectively, T is the Wick's time-ordering operator which has the effect of ordering the operators with the largest time on the left. Here, spin coordinate is omitted for simplicity. For $t_1 > t_2$ ($t_1 < t_2$), $G(\mathbf{r}_1 t_1, \mathbf{r}_2 t_2)$ describes the probability amplitude to find an electron (hole) in $\mathbf{r}_1$ ($\mathbf{r}_2$) at time t_1 (t_2) after an electron (hole) is added in $\mathbf{r}_2$ ($\mathbf{r}_1$) at time t_2 (t_1) to the system in its ground state. The creation of a hole is equivalent to the removal of an electron. By Fourier

transformation, we get the Lehmann representation of one-particle Green's function in the energy space

$$G(\mathbf{r}_1,\mathbf{r}_2;\omega)=\sum_i \frac{f_i(\mathbf{r}_1)f_i^*(\mathbf{r}_2)}{\omega-E_i+i\eta\,\mathrm{sgn}(E_i-\mu)} \tag{2}$$

in terms of energies E_i and Lehmann amplitudes $f_i(\mathbf{r})$ defined by

$$E_i=\begin{cases} E_{N+1,i}-E_{N,0} & if \quad E_i>\mu \\ E_{N,0}-E_{N-1,i} & if \quad E_i<\mu \end{cases} \tag{3}$$

$$f_i(\mathbf{r})=\begin{cases} \langle N,0|\hat{\psi}(\mathbf{r})|N+1,i\rangle & if \quad E_i>\mu \\ \langle N-1,i|\hat{\psi}(\mathbf{r})|N,0\rangle & if \quad E_i<\mu \end{cases} \tag{4}$$

where μ is the chemical potential of the system; η is a positive real infinitesimal introduced to guarantee the convergence of the Fourier transformation; $E_{N,0}$ is the total energy of the system in its ground state; and $|N-1,i\rangle$ ($|N+1,i\rangle$) and $E_{N-1,i}$ ($E_{N+1,i}$) denote the wave function and total energy of the system in the ith state after removal (addition) of an electron. It is evident that E_i corresponds to the ionization energy or electron affinity that is measured by photoemission or inverse photoemission spectroscopies. E_i is also the pole of $G(\mathbf{r}_1, \mathbf{r}_2; \omega)$. Accurate ionization energy and electron affinity can be obtained if accurate one-particle Green's function of the interacting electron system is available.

The full one-particle Green's function cannot be calculated exactly, and therefore one need to employ some approximations. Defining a non-interacting one-particle Green's function $G_0(\mathbf{r}_1, \mathbf{r}_2; \omega)$ for a system where the exchange and correlation effects are turned off leaving only the Hartree term, the interacting one-particle Green's function $G(\mathbf{r}_1, \mathbf{r}_2; \omega)$ is linked to $G_0(\mathbf{r}_1, \mathbf{r}_2; \omega)$ via Dyson's equation[6]

$$G(\mathbf{r}_1,\mathbf{r}_2;\omega)=G_0(\mathbf{r}_1,\mathbf{r}_2;\omega)+\int\int G_0(\mathbf{r}_1,\mathbf{r}';\omega) \times\Sigma(\mathbf{r}',\mathbf{r}'';\omega)G(\mathbf{r}'',\mathbf{r}_2;\omega)d\mathbf{r}'d\mathbf{r}'' \tag{5}$$

Starting from the equation of motion for the fermion creation and annihilation operators in the Heisenberg representation and the representation of one-particle Green's function in Eq. (1), one gets the differential form of Dyson's equation

$$\left[i\frac{\partial}{\partial t_1}-\left(-\frac{\nabla^2}{2}+V_H(\mathbf{r}_1)+V_{ext}(\mathbf{r}_1)\right)\right]G(1,2) -\int d3\Sigma(1,3)G(3,2)=\delta(1,2) \tag{6}$$

Here, integers 1, 2, and 3 are short notations for a combined space and time coordinates, e.g., (1) = ($\mathbf{r}_1$, t_1). V_H and V_{ext} are the Hartree potential and the external potential that accounts for the interaction with the nuclei, respectively. In the QP approximation, one-particle Green's function can be represented by QP energies and wave functions as

$$G(\mathbf{r}_1,\mathbf{r}_2;\omega)=\sum_i \frac{\psi_i^{QP}(\mathbf{r}_1)\psi_i^{QP*}(\mathbf{r}_2)}{\omega-E_i^{QP}} \tag{7}$$

Fourier transforming Eq. (6) to the energy space and inserting Eq. (7), one obtains the QP equation

$$\left[-\frac{1}{2}\nabla^2+V_H(\mathbf{r})+V_{ext}(\mathbf{r})\right]\psi_i^{QP}(\mathbf{r}) +\int\Sigma\left(\mathbf{r},\mathbf{r}';E_i^{QP}\right)\psi_i^{QP}(\mathbf{r}')d\mathbf{r}'=E_i^{QP}\psi_i^{QP}(\mathbf{r}) \tag{8}$$

This equation has a similar form to the single-particle equation in DFT

$$\left[-\frac{1}{2}\nabla^2+V_H(\mathbf{r})+V_{ext}(\mathbf{r})\right]\psi_i^{DFT}(\mathbf{r}) +V_{xc}(\rho(\mathbf{r}))\psi_i^{DFT}(\mathbf{r})=E_i^{DFT}\psi_i^{DFT}(\mathbf{r}) \tag{9}$$

However, solutions of Eq. (8) are QP energies and QP wave functions which are physically more meaningful than the solutions of the Kohn–Sham equation. Except the highest occupied eigenvalue of the Kohn–Sham equation which has been proved to correspond to the negative of the ionization potential physically, solutions of the Kohn–Sham equation are just mathematical tools that ensure the minimization of the density functional and cannot be linked to the electronic structure measured in experiment.[3,19]

It should be mentioned that the QP equation (Eq. (8)) is valid and applicable only when the spectral function A, which is defined as $A(\mathbf{r}_1, \mathbf{r}_2; \omega) = \pi^{-1}|\mathrm{Im}G(\mathbf{r}_1, \mathbf{r}_2; \omega)|$, is composed solely by independent QP peaks. If coupling of electrons to excitations in materials is strong, satellite structures arising from plasmons may appear in the spectral function besides the QP parts.[3,18] This complicated one-particle Green's function should be obtained by solving the Dyson's equation directly through the method like cumulant expansion which has attracted great attention in recent years.[23–28] Nonetheless, QP approximation has proved to be effective and powerful in most cases where effects from satellites can be ignored.

HEDIN'S EQUATION AND GW METHOD

In the language of Green's function, self-energy takes the form

$$\Sigma(1,2) = i\int d34 v(1^+,3)[-G_2(1,3;4,3^+) + G(1,4)G(3,3^+)]G^{-1}(4,2) \quad (10)$$

where v is the bare Coulomb potential, G_2 is the two-particle Green's function, and (1^+) stands for $(\mathbf{r}_1, t_1 + \eta)$. Because it involves many-particle Green's functions, exact determination of the self-energy is very complicated and some approximations have to be resorted to. The simple way is to expand Σ in terms of the bare Coulomb potential v. However, this type of expansion may diverge for metals. Hedin proposed to express Σ as a series of expansion in the screened Coulomb potential W instead, where W is defined as[5,15]

$$W(1,2) = \int v(1,3)\varepsilon^{-1}(3,2)d3 \quad (11)$$

where ε is the dielectric function which measures the screening in the system arising from polarization effects. Its long-wavelength limit at zero frequency is the macroscopic dielectric constant ε_∞. For example, ε_∞ for bulk silicon and diamond are 11.7 and 5.7, respectively. W, representing the effective interaction between two electrons, is weaker than v. If all terms of W are included in the expansion of Σ, exact self-energy can still in principle be calculated from following Hedin's equations

$$\Sigma(1,2) = i\int G(1,4)W(1^+,3)\Gamma(4,2;3)d(3,4) \quad (12)$$

$$W(1,2) = v(1,2) + \int W(1,3)P(3,4)v(4,2)d(3,4) \quad (13)$$

$$P(1,2) = -i\int G(2,3)G(4,2)\Gamma(3,4;1)d(3,4) \quad (14)$$

$$\Gamma(1,2;3) = \delta(1,2)\delta(1,3) + \int\frac{\delta\Sigma(1,2)}{\delta G(4,5)}G(4,6)G(7,5)\times\Gamma(6,7;3)d(4,5,6,7) \quad (15)$$

when the exact one-particle Green's function of the interacting system was known. Hedin's equations and Dyson's equation form a closed set of equations from which self-energy and interacting Green's function can be determined by an iteration process using the scheme shown in Figure 1.

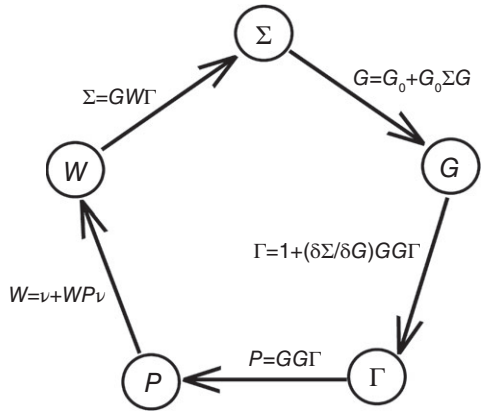

FIGURE 1 | Schematic representation illustrating how the self-energy $\sum$ and one-particle Green's function G can be determined using Hedin's equations and Dyson's equation iteratively.

To simplify the calculations, Hedin introduced the GW approximation where contribution from $\delta\Sigma/\delta G$ in the vertex function Γ is omitted and thus the self-energy operator reduces to

$$\Sigma(1,2) = iG(1,2)W(1^+,2) \quad (16)$$

The irreducible polarizability P is also simplified to

$$P(1,2) = -iG(1,2)G(2,1) \quad (17)$$

which in the energy space takes the form

$$P(\mathbf{r},\mathbf{r}';\omega) = 2\sum_{n\mathbf{k}}^{\text{occ}}\sum_{n'\mathbf{k}'}^{\text{unocc}}\Psi^*_{n\mathbf{k}}(\mathbf{r})\Psi_{n'\mathbf{k}'}(\mathbf{r})\Psi^*_{n'\mathbf{k}'}(\mathbf{r}')\Psi_{n\mathbf{k}}(\mathbf{r}') \times\left\{\frac{1}{\omega - E_{n'\mathbf{k}'} + E_{n\mathbf{k}} + i\eta} - \frac{1}{\omega + E_{n'\mathbf{k}'} - E_{n\mathbf{k}} - i\eta}\right\} \quad (18)$$

where E and ψ are the QP energies and wave functions originating from the Lehmann representation of the one-particle Green's function, the factor 2 accounts for the spin degeneracy. This form of irreducible polarizability is the same as that deduced from the random-phase approximation (RPA). GW approximation in fact corresponds to retain only the first-order term of the expansion of self-energy in terms of the screened Coulomb potential. In practical GW implementations, the screened Coulomb interaction W is calculated by Eq. (11) where the dielectric function can be determined from the irreducible polarizability P by Eq. (18) in advance through the relation

$$\varepsilon(1,2) = \delta(1,2) - \int P(3,2)v(1,3)d3 \quad (19)$$

PROCEDURES AND TECHNIQUES FOR GW CALCULATIONS

The simplest GW calculation is the one-shot GW, or G_0W_0. The standard procedure for it is that: first, an appropriate first-principles technique, usually DFT or less often Hartree–Fock theory (HF), is chosen as the starting point to compute the single-particle eigenvalues and eigenfunctions of the system in its ground state; second, the solutions in the previous step are inserted into Eqs (7), (18), and (19) to construct the one-particle Green's function and dielectric function; third, the screened Coulomb potential and sequentially the self-energy are determined through Eqs (11) and (16), respectively; finally, Eq. (8) is solved to obtain the QP enengies and QP wave functions if applicable. There is no iteration, no update of G and W in G_0W_0. In G_0W_0, single-particle eigenvalues and wave functions from DFT (or HF) are considered as zero-order approximation to the QP ones. QP energies are predicted perturbatively to first order by

$$\begin{aligned} E_i^{QP} &= E_i^{DFT} + \langle \psi_i^{DFT} | \Sigma\left(E_i^{QP}\right) - V_{xc} | \psi_i^{DFT} \rangle \\ &\approx E_i^{DFT} + Z_i \langle \psi_i^{DFT} | \Sigma\left(E_i^{DFT}\right) - V_{xc} | \psi_i^{DFT} \rangle \end{aligned} \quad (20)$$

where Z_i is a renormalization factor to express the dependence of self-energy on QP energy[29]

$$Z_i = \left[1 - \langle \psi_i^{DFT} | \frac{\partial \Sigma(E)}{\partial E}\Big|_{E=E_i^{DFT}} | \psi_i^{DFT} \rangle\right]^{-1} \quad (21)$$

As shown in the first step in Eq. (20), self-energy Σ on the right side of the equal sign is a function of the QP energy E_i^{QP} on the left side. To simplifying the calculation, a further approximation, i.e., the second step in Eq. (20), is usually applied assuming that the self-energy at E_i^{QP} can be expanded to first order in the vicinity of the Kohn-Sham eigenvalue E_i^{DFT} by[29]

$$\Sigma\left(E_i^{QP}\right) \approx \Sigma\left(E_i^{DFT}\right) + \Sigma\left(E_i^{QP} - E_i^{DFT}\right) \frac{\partial \Sigma(E)}{\partial E}\Big|_{E=E_i^{DFT}} \quad (22)$$

Now, the second line in Eq. (20) is only determined by Kohn–Sham eigenvalues and wave functions. Energy derivatives of self-energy in Eq. (22) can be computed by finite difference. Here, only diagonal matrix elements of Σ need to be calculated, while the off-diagonal terms, which represent the mixing of single-particle wave functions, are neglected. Generally, G_0W_0 can lead to good agreement with experiment for QP energies. Sometimes, the performance of G_0W_0 is not satisfactory, and its results are affected by the starting DFT point. This may be improved either by executing self-consistent GW calculations, fully or partially, or by taking high-order contribution to the self-energy, e.g., vertex function, into account.

Evaluation of self-energy involves an integration over the energy

$$\Sigma(\mathbf{r},\mathbf{r}';E) = \frac{i}{2\pi}\int e^{-i\omega\eta} G(\mathbf{r},\mathbf{r}';E-\omega) W(\mathbf{r},\mathbf{r}';\omega) d\omega \quad (23)$$

The dependence of the dynamically screened interaction W on energy is embodied in the dielectric function through Eqs (11), (18), and (19). Dielectric matrices $\varepsilon_{GG'}(\mathbf{q},\omega)$, where $\mathbf{G}$ and $\mathbf{G}'$ are reciprocal lattice vectors and $\mathbf{q}$ the vector in the first Brillouin zone of the reciprocal space, at many values of ω are in principle required to be calculated in order to get a converged value of self-energy. However, full-frequency calculations are expensive in CPU time relatively. An approximated scheme, the plasmon-pole model, is now being widely employed to reduce the number of dielectric matrices calculated explicitly. Furthermore, the plasmon-pole model permits an analytic evaluation of the energy integral in Eq. (23). Plasmon-pole model is based on the observation that the imaginary part of the inverse dielectric matrix is generally a peaked function in ω, so that its real part can be approximated by

$$\mathrm{Re}\ \varepsilon^{-1}_{GG'}(\mathbf{q},\omega) = \delta_{GG'} + \frac{\Omega^2_{GG'}(\mathbf{q})}{\omega^2 - \tilde{\omega}^2_{GG'}(\mathbf{q})} \quad (24)$$

The two parameters $\omega_{GG'}$, pole position, and $\Omega_{GG'}$, pole strength, which are independent of the frequency, can be determined by two constraints including (1) static limit of $\varepsilon^{-1}_{GG'}$ calculated by RPA at the point $\omega = 0$ and (2) $\varepsilon^{-1}_{GG'}$ at another point ω along the imaginary energy axis or the f-sum rule. Several types of plasmon-pole models were proposed, such as Hybertsen–Louie,[29] Godby–Needs,[30] von der Linden–Horsch,[31] and Engel-Farid.[32] The performance of plasmon-pole models were tested recently on some molecules and solids.[33–36]

However, if the structure of $\varepsilon^{-1}(\omega)$ in the frequency domain cannot be properly represented by single poles, or if one is interested in satellites in the spectral function or in QP lifetimes, one needs to evaluate the full-frequency-dependent dielectric matrix. Several schemes have been implemented to carry out full-frequency calculations, including the

analytical continuation method, the direct method, the contour deformation method, and so on.[33–35,37–42] The analytical continuation method requires to compute dielectric matrix $\epsilon(i\omega)$ and self-energy $\Sigma(i\omega)$ on the imaginary energy axis.[39] $\Sigma(i\omega)$ is then analytically extrapolated to the real energy axis using the Padé approximation or a multipole model function. This approach is based on the idea that Σ has no poles and has a smooth shape on the imaginary energy axis in contrast with a ragged shape on the real one so that Σ can be represented more easily with few energy points on the imaginary axis than on the real axis. In the contour deformation method, the integral along the real energy axis is transformed into an integral over an appropriate contour in the complex plane,[43] so that the energy-dependent part of the self-energy, i.e., the correlation part, can be expressed as[42]

$$\Sigma^{C}(E) = -\frac{i}{2\pi}\int_{-\infty}^{\infty} G(E-i\omega)W^{\mathrm{dyn}}(i\omega)d(i\omega) - \sum_{p}\lim_{z\to z_p} G(z)W^{\mathrm{dyn}}(z)(z-z_p) \quad (25)$$

The first term is an integration along the imaginary energy axis. The second term embraces contributions from the poles, z_p, of the one-particle Green's function and the dynamical part of screened interaction $W^{\mathrm{dyn}} = W - \nu$, enclosed inside the contour. Plasmon-pole approximation can also be avoided by the linear-response Sternheimer equation approach as will be described below.

TWO-PARTICLE GREEN'S FUNCTION

Two-particle Green's function is defined as

$$G_2(1,2;1',2') = (-i)^2\langle N,0|T\left[\hat{\psi}(1)\hat{\psi}(2)\hat{\psi}^{\dagger}(2')\hat{\psi}^{\dagger}(1')\right]|N,0\rangle \quad (26)$$

which involves four time variables. Through the ordering of the four times appearing in Eq. (26), two-particle Green's function can describe the propagation of coupled particle–particle, particle–hole, and hole–hole pairs. For the exciton (particle–hole pair), we are interested in here, only the orderings $t_1, t_{1'} > t_2, t_{2'}$ and $t_1, t_{1'} < t_2, t_{2'}$ are considered, while the corresponding two-particle Green's function is rewritten as[22]

$$\begin{aligned} G_2^{exciton}(1,2;1',2') &= -\Theta\left(\tau-\frac{1}{2}|\tau_1|-\frac{1}{2}|\tau_2|\right) \\ &\times\sum_{S}\exp\left[-i\left(E_{N,S}-E_{N,0}\right)\tau\right]\chi_S(\mathbf{r}_1,\mathbf{r}_{1'};\tau_1)\widetilde{\chi}_S(\mathbf{r}_2,\mathbf{r}_{2'};\tau_2) \\ &-\Theta\left(-\tau-\frac{1}{2}|\tau_1|-\frac{1}{2}|\tau_2|\right) \\ &\times\sum_{S}\exp\left[i\left(E_{N,S}-E_{N,0}\right)\tau\right]\widetilde{\chi}_S(\mathbf{r}_1,\mathbf{r}_{1'};\tau_1)\chi_S(\mathbf{r}_2,\mathbf{r}_{2'};\tau_2) \end{aligned} \quad (27)$$

where $E_{N,S}$ is the total energy of the system in the excited state S, $E_{N,S} - E_{N,0}$ is the excitation energy, i.e., exciton energy is the pole of two-particle Green's function, and χ_S is the exciton wave function (or -particle–hole amplitude)

$$\chi_s(1,1') = \langle N,0|T\left[\hat{\psi}(1)\hat{\psi}^{\dagger}(1')\right]|N,s\rangle \quad (28)$$

BETHE–SALPETER EQUATION

The motion of two-particle Green's function obeys the BSE

$$\begin{aligned} L(1,2;1',2') &= G(1,2')G(2,1') \\ &+\int G(1,3)G(3',1')K(3,4';3',4)L(4,2;4',2')d(3,3',4',4) \end{aligned} \quad (29)$$

where $L(1, 2; 1', 2')$ is the two-particle correlation function defined as

$$L(1,2;1',2') = -G_2(1,2;1',2') + G(1,1')G(2,2') \quad (30)$$

$K(3, 4'; 3', 4)$ is the two-particle (electron–hole here) interaction kernel which, under GW approximation and assuming $\delta W/\delta G \approx 0$, can be expressed as

$$\begin{aligned} K(3,4';3',4) &= \frac{\delta[V_H(3)\delta(3,3')+\Sigma(3,3')]}{\delta G(4,4')} \\ &= -i\delta(3,3')\delta(4^{+},4')v(3,4) \\ &+i\delta(3,4)\delta(3',4')W(3^{+},3') \end{aligned} \quad (31)$$

It consists of two contributions, the exchange term and the direct term which result from the bare Coulomb potential v and the screened Coulomb potential W, respectively. For the case of $t_1, t_{1'} > t_2, t_{2'}$, and using the QP wave functions to expand the exciton wave functions, i.e.,

$$\chi_S(\mathbf{r},\mathbf{r}') = \sum_{c,v} A_{vc}^{S}\psi_c(\mathbf{r})\psi_v^{*}(\mathbf{r}') \quad (32)$$

the BSE turns into an eigenvalue problem[13,17,44]

$$(E_c - E_v)A^S_{vc} + \sum_{v'c'} K^{AA}_{vc,v'c'}(\Omega_S)A^S_{v'c'} = \Omega_S A^S_{vc} \quad (33)$$

with

$$K^{AA}_{vc,v'c'}(\Omega_S) = \langle c,v'|v|v,c'\rangle + \left(-\frac{i}{2\pi}\right) \times \int_{-\infty}^{+\infty} d\omega \exp(-i\omega\gamma)\langle c,v'|W(\omega)|c',v\rangle \times \left[\frac{1}{\Omega_S - \omega - (E_{c'} - E_v) + i\eta} + \frac{1}{\Omega_S + \omega - (E_c - E_{v'}) + i\eta}\right] \quad (34)$$

where the eigenvalue Ω_S is the exciton energy, c (v) denotes the conduction (valence) band, and γ is a positive real infinitesimal. The first term of Eq. (33) describes the uncorrelated electron–hole pair, while the second term accounts for the interaction between the bound electron–hole pair. The Hamiltonian of Eq. (33) is a function of its eigenvalue. Its solution requires self-consistent calculations. Practical implementation usually only considers the static limit to the BSE Hamiltonian by neglecting the dynamical screening effects arising from terms $\Omega_S - (E_{c'} - E_v)$ and $\Omega_S - (E_c - E_{v'})$.

When the orderings $t_1, t_{1'} > t_2, t_{2'}$ and $t_1, t_{1'} < t_2, t_{2'}$ are taken into account simultaneously, the BSE turns into a set of coupled eigenvalue equations[45]

$$\begin{cases} (E_c - E_v)A^S_{vc} + \sum_{v'c'} K^{AA}_{vc,v'c'}(\Omega_s)A^S_{v'c'} \\ \quad + \sum_{v'c'} K^{AB}_{vc,v'c'}(\Omega_s)B^S_{v'c'} = \Omega_S A^S_{vc} \\ (E_c - E_v)B^S_{vc} + \sum_{v'c'} K^{BB}_{vc,v'c'}(\Omega_s)B^S_{v'c'} \\ \quad + \sum_{v'c'} K^{BA}_{vc,v'c'}(\Omega_s)A^S_{v'c'} = -\Omega_S B^S_{vc} \end{cases} \quad (35)$$

with the exciton wave function expressed as

$$\chi_S(\mathbf{r},\mathbf{r}') = \sum_{c,v} \left[A^S_{vc}\psi_c(\mathbf{r})\psi^*_v(\mathbf{r}') + B^S_{vc}\psi_v(\mathbf{r})\psi^*_c(\mathbf{r}')\right] \quad (36)$$

In Eq. (35), the off-diagonal blocks $K^{AB}_{vc,v'c'}$ and $K^{BA}_{vc,v'c'}\left(= -\left[K^{AB}_{vc,v'c'}\right]^*\right)$ represent the coupling between the resonant ($v \to c$) and antiresonant ($c \to v$) transitions. Equation (35) is usually called the full BSE form, while Eq. (33) is referred to as the Tamm–Dancoff approximation (TDA) to BSE. This concept and the form of equations are similar to those in time-dependent DFT (TDDFT).

In practical BSE calculations, single-particle orbitals from DFT are used to set up the basis sets for exciton wave functions; energies of the occupied and unoccupied orbitals appearing in the first term of Eq. (33) are corrected by GW method; the exchange term of the electron–hole interaction kernel can be calculated accurately, while the plasmon-pole model is usually applied in the direct term where an integration over the energy is involved as shown in Eq. (34). A typical BSE implementation follows the DFT→GW→BSE procedure. In order to reduce the computational cost, sometimes, especially for periodically systems where a large number of wave verctors $\mathbf{k}$ in the first Brillouin zone are demanded to represent the exciton wave functions, the GW step is skipped but instead a rigid energy shift, whose value is determined by separate GW calculations for one or several $\mathbf{k}$ points, is exerted on the occupied or unoccupied DFT single-particle energies.

CODES FOR GW AND BSE CALCULATIONS

The early success and excellent performance of GW method and BSE in QP structures and optical spectra and the increasing demand for state-of-the-art first-principles techniques to understand solar energy conversion and excited-state dynamics process in materials and molecules triggered the rapid development of related methodology and *ab initio* codes. Most of the codes use plane waves as basis sets, some use localized orbitals including Gaussian orbitals,[38,45–49] numerically atomic orbitals,[50] while some employ mixed orbitals, such as the linearized augmented-plane-wave method,[51,52] the linearized muffin-tin orbitals,[53] the projected Wannier functions augmented by numerical atomic orbitals,[54] a linear combination of plane waves and numerical atomic orbitals.[55] Localized orbitals are convenient for all-electron calculations to treat compounds containing transition-metals and to interpret X-ray absorption.[56,57] Some codes have been open to the public and are available freely or commercially, such as BerkeleyGW,[58] ABINIT,[59] yambo,[60] exciting,[51] West,[61] VASP,[62] FHI-aims,[50] and so on. GW method has also been implemented into the quantum chemistry package TURBOMOLE.[49] There are some other codes that have been announced in the literatures, such as Fiesta,[63] SPEX,[52] GPAW,[54] and SaX.[64] Here we just list part of them for reference. Many

researchers have done great contribution to the development of GW and BSE methods.

TECHNIQUES WITHIN GW AND BSE

To make the computation practicable and capable to treat large systems, some approximations are introduced in routine GW and BSE calculations. Early reviews by Aryasetiawan and Gunnarsson,[18] Aulbur et al.,[19] and Onida et al.[3] have discussed some of them. Here we present some new progresses on these respects in recent years.

Self-Consistency in GW

G_0W_0 has achieved great success for the determination of electronic structure. Its agreement with experimental spectra outperforms DFT greatly. It is evident that the starting point (DFT vs HF or DFT with different exchange-correlation functionals) of G_0W_0 may affect the results. The solution to eliminate this effect is to implement self-consistent GW calculations (scGW). The conventional scGW comprises full scGW and partial scGW. In full scGW, eigenvalues and eigenfunctions in G and W are all updated. It has been widely accepted that the results from scGW are even worse than G_0W_0 for homogeneous electron gas and semiconductors potassium and Si.[19] Recent development in algorithm and some benchmark work on solids and molecules seem to give some more promising results, although there is still much controversy.

In 2010, Rostgaard et al. tested full scGW on the ionization potential (IP) of 34 small molecules including LiH, CH_4, SO_2, and so forth.[54] They stated that G_0W_0 with HF as the starting point (G_0W_0-HF) and full scGW underestimate IP by 0.4 and 0.5 eV on average with respect to experiment, respectively. G_0W_0-HF is better than the full scGW a little bit. Koval et al. computed IP of sixteen small molecules most of which are the same as Rostgaard et al.[54] and compared the GW values with those obtained from coupled-cluster calculations CCSD(T) in 2014.[65] They claimed that full scGW shows a small improvement (0.06 eV) with respect to G_0W_0-HF on average. However, the trend of full scGW and G_0W_0-HF is different in their calculations, full scGW underestimates by 0.22 eV but G_0W_0-HF overestimates by 0.28 eV with respect to CCSD(T) on average. Caruso et al. studied the same set of molecules as Rostgaard et al.[54] in 2012 and got a conflicting conclusion.[66] They argued that full scGW improves IP systematically compared to G_0W_0-HF. Full scGW and G_0W_0-HF deviate from the experiment by 2% and 4%, respectively. Subsequently, Caruso et al. further substantiated their point of view by studying five kinds of organic molecules including thiophene, benzothiazole, thiadiazole, naphthalene and tetrathiafulvalene.[41] They found that the average error of full scGW on IP is 0.4 eV, much smaller than that of G_0W_0-HF which is 0.7 eV. They also found that G_0W_0 based on PBE0, i.e., using DFT with the PBE0 hybrid exchange-correlation functional as the starting point, performs even better than full scGW and suggested it to be the optimal technique for QP calculations. According to Caruso's explanation, HF produces too large HOMO–LUMO gap due to the missing of correlation energy and thus leads to an underestimated screening in the Coulomb interaction. PBE, another widely-used exchange-correlation functional in DFT, overestimates the screening on the contrary due to the too small HOMO–LUMO gap calculated, while PBE0 gives a good compromise and is the optimal choice.[41]

There are some attempts in applying the conventional scGW in solids. For example, Ku and Eguiluz argued that full scGW outperforms G_0W_0 and could converge the absolute gap of Si and Ge to 0.1 eV.[67] Full scGW also improves the description of ground-state properties of solid like equilibrium lattice constant and bulk modulus compared to G_0W_0 as demonstrated by Kutepov et al. for Na, Al, and Si using the Galitskii–Migdal formula to evaluate the exchange-correlation part of total energy.[68] The performance of partial scGW was also tested. In the study of some semiconductors and insulators by Shishkin and Kresse,[69] partial scGW where only eigenvalues in G are updated leads to better agreement with experiment than G_0W_0 with DFT-PBE as the starting point (G_0W_0-PBE), while partial scGW where eigenvalues in G and W are both updated gives too large band gaps. Jiang reviewed the self-consistency issue in GW method and its application in *d*/*f*-electron systems like NiO, MnO, and VO_2.[70]

One important advance in scGW is the so-called QP self-consistent GW approximation (QSGW) proposed by van Schilfgaarde et al. in 2006 which has attracted widely attention.[53,71] GW approximation, whether G_0W_0 or scGW, essentially is a perturbation theory where the $\Sigma(\omega) - V_{xc}$ is regarded as first-order perturbation to the single-particle eigenvalue. The smaller this perturbation is, the closer the single-particle eigenvalue to the real QP energy is. The core of the QSGW technique is to find out an optimized effective potential V^{eff} for the single-particle Hamiltonian $H^0 = -\nabla^2/2 + V^{eff}$ through an iterative procedure so that the

perturbation is minimized. Its starting point is also DFT where

$$V^{eff} = V_{ext} + V_H + V_{xc} \quad (37)$$

After a one-shot GW calculation based on this effective potential, a new potential is got

$$V^{GW}(\omega) = V_{ext} + V_H + \Sigma(\omega) \quad (38)$$

The difference $\Delta V(\omega) = V^{GW}(\omega) - V^{eff}$ is a perturbative correction to the effective potential V^{eff}. If $\Delta V(\omega)$ is large, construct a new exchange-correlation potential based on (ω)

$$V_{xc} = \frac{1}{2}\Sigma_{ij}|\Psi_i\rangle\left\{\mathrm{Re}[\Sigma(\varepsilon_i)]_{ij} + \mathrm{Re}\left[\Sigma\left(\varepsilon_j\right)\right]_{ij}\right\}\langle\Psi_i| \quad (39)$$

and insert it into Eq. (37) to construct a new effective potential V^{eff} for H^0. After that, repeat these steps until $\Delta V(\omega)$ is small enough according some criterion and thus the self-consistency is achieved. QSGW does systematically improve the agreement with experiment compared to G_0W_0 as illustrated by van Schilfgaarde et al. for tens of solids including alkali metals, semiconductors, wide band gap insulators, transition metals, transition metal oxides, magnetic insulators and rare earth compounds. This method has been tested on many systems and been used as a standard to develop new algorithms in some groups.[48,72–75] However, QSGW overestimates the band gaps and the error can be large for small-gap materials. Shishkin et al.[73] and Botti and Marques[75] put forward that inclusion of vertex function in the screened Coulomb interaction W and consideration of the lattice polarization in the dielectric function can shrink the QSGW band gap and lead to a better agreement with experiment. Although implementing self-consistency and these high-order effects may improve the precision of GW method, it is impractical for large-size systems presently due to the complicated procedure and prohibitive computational cost. G_0W_0 with a suitable starting single-particle point is a realistic compromise.

Algorithms to Speed up GW

Self-energy can physically be separated into two parts, the exchange or HF contribution Σ^X and the energy-dependent correlation contribution Σ^C which has an expression[19]

$$\Sigma^C(\mathbf{r},\mathbf{r}';E) = \sum_i^{\mathrm{occ}}\sum_{m\neq 0}\frac{V_m(\mathbf{r})V_m^*(\mathbf{r}')\Psi_i(\mathbf{r})\Psi_i^*(\mathbf{r}')}{E+\epsilon_m-E_i-i} + \sum_i^{\mathrm{unocc}}\sum_{m\neq 0}\frac{V_m(\mathbf{r})V_m^*(\mathbf{r}')\Psi_i(\mathbf{r})\Psi_i^*(\mathbf{r}')}{E-\epsilon_m-E_i+i\eta} \quad (40)$$

where $V_m(\mathbf{r}) = \int(\mathbf{r},\mathbf{r}')n_m(\mathbf{r}')d\mathbf{r}'$ is the fluctuation potential induced by the excitation m with energy $\epsilon_m = E_{N,m} - E_{N,0}$ and oscillator strength n_m in the N-electron system, i denotes the single-particle state. Evaluation of dielectric function, and Σ^C involves infinite summations over both occupied and unoccupied single-particle states. This is a major bottleneck in GW and BSE calculations. In practical calculations, summation over unoccupied states is truncated above a certain energy which parameter is determined by convergence tests. The convergence behavior of QP energy and band gap with respect to the number of unoccupied states taken into account is a critical issue in GW runs which has been discussed in many articles and should be checked carefully in calculations. Extreme slow convergence has been encountered when using plane wave approach to treat systems like ZnO[34,69,76–78] and TiO_2[35] which contain strongly localized semicore d states and molecules[79,80] which require large vacuum gap to eliminate interaction between images in repeated supercells. Even if the convergence is perfect as we wish, computational load is still prohibitive for large systems, limiting the application of GW and BSE. There have been some proposals to relieve this problem in the explicit sum-over-states procedure, e.g., the effective-energy technique where only occupied states appear in the summation,[78,81] the simple approximate physical orbital approach where the unoccupied orbitals are replaced by some symmetrized plane waves and localized basis DFT orbitals.[79]

An alternative approach, the linear-response Sternheimer equations within the density-functional perturbation theory, was adopted in some groups to compute the dielectric function.[61,82–87] In this technique, determination of the dielectric function starts from the Sternheimer equation

$$\left(\hat{H}-E_v\pm\omega\right)\Delta\Psi^{\pm}_{v[\mathbf{r},\omega]} = -\left(1-\hat{P}_{occ}\right)\Delta V_{[\mathbf{r},\omega]}\Psi_v \quad (41)$$

where $\hat{H}$ is the effective single-particle Hamiltonian within DFT, $\hat{P}_{occ} = \Sigma_v|\psi_v\rangle\langle\psi_v|$ is the projector on the occupied (valence, v) states, $\Delta\psi^{\pm}_{v[\mathbf{r},\omega]}$ are the variations of single-particle wave functions responding to the

perturbation $\Delta V_{[\mathbf{r},\omega]} = v(\mathbf{r}, \mathbf{r}')$. The dielectric function is thus obtained by

$$\varepsilon(\mathbf{r},\mathbf{r}',\omega) = \delta(\mathbf{r},\mathbf{r}') - \Delta n_{[\mathbf{r},\omega]} \tag{42}$$

where $\Delta n_{[\mathbf{r},\omega]}$ is the change of the density matrix

$$\Delta n_{[\mathbf{r},\omega]} = 2\sum_{v} \psi_v^* \left(\Delta\psi^{+}_{v[\mathbf{r},\omega]} + \Delta\psi^{-}_{v[\mathbf{r},\omega]} \right) \tag{43}$$

This approach does not require the summation over unoccupied states but instead solves self-consistently the linear equation Eq. (41) which involves only the occupied states. If setting $\Delta V_{[\mathbf{r},\omega]}$ to

$$\Delta V_{[\mathbf{r},\omega]} = v(\mathbf{r},\mathbf{r}') + \int \Delta n_{[\mathbf{r},\omega]}(\mathbf{r}'') v(\mathbf{r}'',\mathbf{r}') d\mathbf{r}'' \tag{44}$$

the screened Coulomb interaction W can also be calculated by solving Eq. (41) self-consistently,[61,83,84] without the need to invert dielectric matrics. In the scheme of Giustino et al.,[83,84] one-particle Green's function is obtained by the linear equation

$$\left(\hat{H} - \omega - i\eta\right) G(\mathbf{r},\mathbf{r}';\omega) = -\delta(\mathbf{r},\mathbf{r}') \tag{45}$$

In the work by Galli et al.,[61,88,89] the correlation interaction Σ^C is evaluated by the integration in the imaginary frequency domain

$$\langle \psi_n | \Sigma_c(i\omega) | \psi_n \rangle = \frac{1}{2\pi} \sum_{i,j=1}^{N_{\text{eig}}} \int d\omega' \bar{c}_{ij}(i\omega') \left\langle \psi_n\left(v^{\frac{1}{2}}\Phi_i\right) \left| \left[\hat{H} - i(\omega - \omega')\right]^{-1} \right| \psi_n\left(v^{\frac{1}{2}}\Phi_j\right) \right\rangle \tag{46}$$

where Φ is the eigenvectors of the inverse of the Hermitian dielectric matrix $\tilde{\varepsilon} = v^{-1/2}\varepsilon v^{1/2}$, N_{eig} is the parameter to truncate the summation which is determined through convergence tests, $\bar{c}_{ij}$ is the expansion coefficients of the polarizability in terms of Φ. The integration in Eq. (46) is realized by the Lanczos-chain algorithm,[90] and the self-energy in the real frequency domain is then computed by analytical continuation methods.[91] Lanczos-chain algorithm has also been employed by Umari et al. with localized Wannier-type orbitals to represent the polarizability.[92,93] In the approaches by Galli, Giustino and Umari et al., not only the summation over unoccupied states but also the plasmon-pole approximation are avoided. There are other proposals raised recently to increase the efficiency of GW method, such as the LDA + GdW method by Rohlfing,[94] the stochastic GW method by Neuhauser et al.,[95] and so on.

Another crucial issue that influence the speed of GW calculation is the basis set. In the realization of GW approach, the irreducible polarizability is expanded in the form of

$$P(\mathbf{r},\mathbf{r}';\omega) = \sum_{\alpha\beta} \varphi_\alpha(\mathbf{r}) P_{\mu\nu}(\omega) \varphi_\beta(\mathbf{r}') \tag{47}$$

where $\varphi_i(\mathbf{r})$ are elements of the basis. Convergence of the plane wave basis can be systematically controlled by a single parameter—energy cutoff. However, in the study of bulk ZnO and monolayer MoS_2, Shih et al. and Qiu et al. found that the convergence behavior of energy cutoff and the number of unoccupied orbitals in the summation as discussed above are strongly correlated.[76,96] Advantage of localized basis set is the high efficiency, however the control of its completeness and convergence is not an easy task. Some literatures have discussed this issues for basis sets composed by Gaussian orbitals, numerically atomic orbitals, and so forth.[38,40,46,47,54,92,97]

TDA and Dynamical Electron–Hole Interaction

TDA is the default choice in routine BSE calculations. The reliability of TDA was verified by Sander et al. recently for solids including Si, C, and LiF.[98] In 2009, Grüning et al. and Ma et al. found that TDA may break down for confined systems such as nanotubes and organic molecules where the electron density is strongly inhomogeneous and/or the exchange interaction between electron and hole is huge.[99–101] For instance, TDA induces a 2 eV error in the photoabsorption peak of the single-walled carbon nanotube and a 0.4∼0.5 eV error in the excitation energy of the lowest $\pi \rightarrow \pi^*$ transition for biological chromophore molecules. In these molecules, the coupling between the resonant–antiresonant transitions originates predominantly from the exchange term, contribution from the direct term is minor relatively. Later on, the overestimation of TDA on excitation energy is observed in more organic molecules, e.g., thiophene,[102–104] DNA and RNA nucleobases,[105] bacteriochlorin,[106] dyes,[63,107,108] chromophores,[109,110] dipeptide,[111] copper enzymes,[112,113] and so on. The effect of TDA is not important for all the excited states. For some dark states, for example the $n \rightarrow \pi^*$ transition in photoactive yellow proteins[100] and DNA nucleobases[105], the long-range charge-transfer excitations,[105,106] the error induced by TDA is nearly zero. However, to get an accurate picture for the entire excitation spectrum,

full BSE is required instead of its TDA simplification. In the work of Conte et al., BSE-TDA and full BSE were found to give qualitatively different photoisomerization pathways for the retinal protonated Schiff base.[110]

In principle, BSE Hamiltonian is the function of its eigenvalues through the electron–hole interaction kernel K. This dependence is usually not taken into account in practical calculations based on the assumption that the dynamical screening effects in the electron–hole interaction kernel are small and negligible when the excitonic binding energy $\Omega_S - (E_c - E_v)$ is much smaller than the plasma frequency. In the work on organic molecules, it is found that dynamical electron–hole screening effects are strong for some kinds of excitations. For example, dynamical screening effects redshift the excitation energies of $n \rightarrow \pi^*$ transitions in photoactive yellow proteins and DNA nucleobases by 0.3 eV.[100,102,105] Marini and Del Sole also demonstrated that dynamical excitonic effects are crucial for the optical absorption in bulk copper, silver and silicon.[114]

Excited-State Force

Optical absorption can lead to structural variation which may trigger subsequent processes like photochemical reaction, photoluminescence, energy transfer, carrier separation, charge transfer, and so forth. In quantum chemistry methods like TDDFT, CIS, and EOM-CCSD, excited-state force can be calculated analytically.[115,116] Within the GW + BSE scheme, analytical excited-state forces are still unavailable. However, in 2003 Ismail-Beigi and Louie proposed an approximate approach to evaluate the excited-state force.[117] According to their theory, within TDA the derivative of the excitation energy with respect to the ionic coordinate R is

$$\partial_R \Omega_S = \sum_{vc,v'c'} A^{S*}_{vc} A^{S}_{v'c'} \partial_R H^{BSE}_{vc,v'c'} \tag{48}$$

where

$$\partial_R H^{BSE}_{vc,v'c'} = \left(\partial_R E^{QP}_c - \partial_R E^{QP}_v\right)\delta_{cc'}\delta_{vv'} + \partial_R K_{vc,v'c'} \tag{49}$$

The derivatives of QP energies are approximated by their DFT counterparts, i.e., assuming that the QP correction $\Sigma - V_{xc}$ is a constant and independent of orbitals and structures. Based on the basic assumption $\delta W/\delta G \approx 0$ in the derivation of the electron–hole interaction kernel K, the second term in Eq. (49) can be expressed as

$$\partial_R K_{vc,v'c'} = \sum_j \left[P^R_{jv} K_{jc,v'c'} + P^{R*}_{jc} K_{vj,v'c'} + P^{R*}_{jv'} K_{vc,jc'} + P^R_{jc'} K_{vc,v'j}\right] \tag{50}$$

with $P^R_{ji} \equiv \langle j|\{\partial_R|i\rangle\}$ which is calculated by first order perturbation theory

$$P^R_{ji} = \begin{cases} 0 & if\ E_i = E_j \\ \dfrac{\langle j|\partial_R \hat{H}|i\rangle}{E_i - E_j} & if\ E_i \neq E_j \end{cases} \tag{51}$$

where $\hat{H}$ is the single-particle Hamiltonian within DFT. Quantities in the first term of Eq. (49) are determined by $\partial_R E_i = \langle i|\partial_R \hat{H}|i\rangle$. $\partial_R \hat{H}$ is computed by density functional perturbation theory. Ismail-Beigi and Louie employed their approach to explore the formation process of self-trapped excitons in silicon dioxide.[118]

Others

There are some extensions of the GW and BSE methods to treat specific systems and to investigate phenomena beyond just the energies of QPs and excitons. Organic molecules are usually embedded in some environments, such as protein, water solution, and so on. It is critical to understand how the environment tunes the optical properties of organic molecules. The most popular way to include the environmental effects in first-principles calculations is the Quantum Mechanics/Molecular Mechanics (QM/MM) scheme. Conte et al. combined GW + BSE and QM/MM approaches and investigated the influence of water solution on the optical absorption of indole.[119] By applying Baer's diabatization scheme within the GW + BSE method, Kaczmarski et al. studied the nonadiabatic effects in the photoisomerization reaction process of the protonated Schiff-base retinal chromophore.[120] Lischner et al. proposed an approach within the GW method to deal with QP excitations in open-shell systems like molecules NO_2, O_2, NF_2, ClO_2, and the negatively charged nitrogen-vacancy center in bulk diamond.[121] Aryasetiawan and Biermann generalized the Hedin's equations to systems containing spin-orbit and spin-spin interactions, and derived the corresponding spin-dependent GW method.[122] This method was employed in calculating electronic structures of Hg chalcogenides HgS, HgSe, and HgTe,[123] topological insulators Bi_2Se_3 and Bi_2Te_3,[124] and light actinides Np, U, and Pu.[125]

By taking electron–phonon interaction into account in the self-energy operator through the Heine-Allen-Cardona theory, Marini et al. and Giustino et al. uncovered the important role of temperature and zero-point atomic motion in the electronic structure and optical absorption of bulk Si, diamond, hexagonal BN and trans-polyacetylene.[126–129] In these studies, the electron–phonon coupling strength, which is closed related to the derivative of potential with respect to ionic positions, is computed at the DFT-LDA level. In the calculation of excited-state forces by Ismail-Beigi and Louie as discussed in previous section, derivatives of QP energies with respect to ionic positions are also approximated by their DFT-LDA counterparts. Nevertheless some researches illustrate that DFT within LDA and GGA significantly underestimates the electron–phonon coupling strength, the first- and second-order derivatives of single-particle energies. The gap between experiments and theoretical studies by DFT can be cured when using self-energy and QP energies at the GW level to produce the derivatives.[130–134] This is crucial to explain the origin of superconductivity in materials.

APPLICATIONS

DFT and TDDFT are the most popular and efficient first-principle approaches to compute electronic structures and excited states nowadays. However, it is well known that their results are heavily affected by the exchange-correlation functionals which contain some empirical parameters. Quantum chemistry methods, such as quantum Monte Carlo, coupled-cluster, complete-active second-order perturbation theory (CASPT2), can achieve high accuracy, but their usage is limited to small molecules due to the unfavorable scaling with the system size (> N^6, where N is the number of basis functions) and they are also difficult to be applied in periodic systems like solids, one- or two-dimensional nanomaterials. The ability of GW and BSE methods to compute electronic structures and excited states without empirical parameters, with appealing scaling (~N^4) and with comparable accuracy to the high-level quantum chemistry methods, together with the development of computational facilities and *ab initio* GW + BSE codes, boosts its applications during the last years greatly.[3,117,135] The performance of GW and BSE methods in solids have been demonstrated and discussed in a large number of literatures and previous reviews.[3,19,71] In this section, we give a brief overview on some recent applications in solids, molecules and nanomaterials.

A lot of attention has been paid to crystals like TiO_2, $CuIn(S,Se)_2$, $CH_3NH_3PbI_3$ which are important materials used in solar cells, photocatalysis, hydrolysis, and so on. Two experimental groups measured the electronic band gap of rutile TiO_2 to be 3.3 and 3.6 eV, respectively. Using DFT-PBE as the starting point and employing the plasmon-pole model (PPM), Chiodo et al. calculated the G_0W_0 band gap of rutile TiO_2 to be 3.59 eV as compared to the 1.93 eV PBE gap.[136] The QSGW gap from van Schilfgaarde et al. is 3.78 eV.[71] As presented in the previous section, QSGW overestimates the band gap overall. Kang and Hybertsen compared the G_0W_0 gap of rutile TiO_2 obtained by the full-frequency procedure (3.38 eV), Hybertsen–Louie PPM (4.27 eV) and von-der-Linden–Horsch PPM (3.70 eV) with DFT-LDA as the starting point, claiming that full frequency dependence of the dielectric matrix should be considered for TiO_2.[35] Localized *d* electrons play a crucial role in compounds containing transition metals. Using self-consistent COHSEX (a static approximation to GW) calculations to optimize the starting point of G_0W_0, Vidal et al. resolved the dispute over the band gap of $CuIn(S,Se)_2$ and also pointed out that, to give a correct dependence of the band gap on the structure of $CuIn(S,Se)_2$ by DFT using the Heyd–Scuseria–Ernzerhof (HSE06) hybrid exchange-correlation functional, the parameter in HSE06 which controls the amount of Fock exchange must vary proportionally to the electronic screening.[137] In the study of $CH_3NH_3PbI_3$, Filip and Giustino, and Brivio et al. obtained the band gap which is in good agreement with experiment after performing self-consistent GW calculations.[138,139]

Water plays a central role in many chemical and biological processes and energy conversion. Yet, its electronic properties and excited states are still poorly understood. Using a model function to describe the dielectric screening, Hahn et al. evaluated the first optical absorption peak of H_2O molecule to be at 7.2 eV by GW + BSE, in excellent agreement with the experimental value of 7.4 eV.[140] Their theoretical optical absorption spectrum of hexagonal ice is also consistent with the experiment. Through comparison with DFT employing PBE, PBE0 and HSE06 hybrid functionals, Pham et al. showed that the use of GW method is crucial to obtain electronic structures of liquid water that agree with experiment.[141] HSE06 and PBE0 underestimate the band gap by 2.7 and 2.0 eV, respectively. Pham et al. used a large unit cell containing 64 water molecules to simulate the liquid water. Swartz and Wu analyzed the impact of solvent water molecules and proton transfer on the ionization potential

distributions of OH^- and H_3O^+ using a unit cell consisting of 63 water molecules and the ions, and reproduced the main features in the experimental photoemission spectroscopy.[142] GW method was also employed to analyze the x-ray absorption spectra of liquid water by Kong et al.[143]

The interface between molecules and solids has been intensely studied due to its pivotal role in various applications. Wang et al. investigated the fast decay process of the electron–hole pair created in the absorbed CO molecule initially into the MgO substrate and demonstrated that the charge-transfer excitonic state between CO and MgO facilitates the decay.[144] The HOMO–LUMO gap of benzene molecule reduces from 10.5 eV in the gas phase to 7.2 eV on the graphite surface because of the polarization effects from the substrate.[145] Electronic screening from Al(111) surface lowers the energy of charge-transfer excitations in molecular complexes such as benzene–tetracyanoethylene by up to 1 eV from GW + BSE calculations, while TDDFT fails to describe this phenomenon.[146] Electronic level alignment of water and organic molecules on semiconductor substrates was investigated by several groups with GW method, for example by Migani et al. for water on TiO_2(110) surface,[147,148] by Pham et al. for water on Si(111) surface,[149] by Kharche et al. for water on GaN and ZnO $(10\bar{1}0)$ surface,[150] by Patrick and Giustino for the chromophore molecule $Ru(dcbpyH_2)_2(NCS)_2$ and by Verdi et al. for the dye molecule (4-diphenylamino)phenylcyanoacrylic acid on TiO_2(101) surface.[151,152] In these molecule–solids interface calculations, the systems are usually large. For example, Pham et al. used 108 water molecules and 72 silicon atoms in their models, Patrick and Giustino's model consists of 299 atoms.

GW + BSE approach is also adopted in the study of excitonic effects in one- and two-dimensional materials like carbon nanotubes, graphene, phosphorene, monolayer MoS_2, $MoSe_2$, Sb_2S_3, and so on.[96,153–156] The first optical absorption peaks of the (5, 0) and (3, 3) single-walled carbon nanotubes are calculated to be 1.33 and 3.17 eV which agree very well with the experimental values of 1.37 and 3.1 eV, respectively.[157] Rohlfing clarified the mechanism of exciton redshifts in carbon nanotubes caused by the environment such as nearby carbon nanotube and other physisorbates.[158] GW + BSE calculations help understanding the modulation of optical conductivity in graphene by electron and hole doping.[159]

In 2001, Grossman et al. assessed the performance of GW and BSE methods on molecules and illustrated the excellent agreement of these methods with quantum Monte Carlo approach and experiment, while the GW and BSE methods are more efficient than quantum Monte Carlo numerically.[135] Some benchmark work of GW and BSE on molecules are presented recently in several literatures. In the study on 39 small molecules containing transition atoms and 7 molecules for photovoltaics using the Gaussian-orbital-based code Fiesta, Körbel et al. demonstrated that the accuracy of G_0W_0-PBE0 on ionization energy, electron affinity and HOMO–LUMO gap can reach 0.3, 0.3, and 0.1 eV, respectively, with respect to experiment.[160] The accuracy of BSE with PBE0 as the starting point is about 0.3 eV. Jacquemin et al. conducted an extensive benchmark calculations for 28 organic molecules of the Thiel's set and 13 dye molecules using the Fiesta package.[161] G_0W_0 with PBE0 as the starting point may lead to an average error of 0.59 eV compared to the reference calculations by CCSD, while self-consistent iteration in GW by updating the QP energies only can improve the results substantially. Compared to TDDFT, GW + BSE is not only parameter-free but also suitable to a wide range of systems and capable to describe any kind of excitations including Frenkel, Wannier and charge-transfer ones effectively. Charge-transfer excitation, especially the intermolecular ones, is involved in excited-state dynamics process of many kinds of organic systems. Duchemin et al. and Yin et al. successfully positioned the energies of charge-transfer excitations in zincbacteriochlorin–bacteriochlorin complex and DNA molecules in aqueous solution by GW + BSE, respectively.[105,106] GW + BSE was also applied in describing charge-transfer excitations in organic molecular crystals like thiophene,[102,162] pentacene,[163,164] rubrene,[165] 3,4,9,10-perylene tetracarboxylic dianhydride,[166] and polyacetylene.[167]

CONCLUSION AND OUTLOOK

The last three decades saw the rapid development of GW method and BSE. Their achievements in a variety of systems indicate that they are promising first-principles approaches to meet the growing demand in electronic excited states calculations for both periodic and nonperiodic systems. The current precision of the typical G_0W_0 with a suitable starting single-particle point and the BSE calculations based on it is satisfactory based on their comparison with other high-level quantum chemistry approaches and experiment. It seems that it will not be too far to see their widely applications in material and molecular science. More efforts are still needed to expand the

functions of GW and BSE methods and to improve their efficiency for large complex systems. For example, analytic approach is unavailable yet to evaluate the first-order energy derivatives of excited states which is useful to simulate structural changes in response to photon irradiation; open-shell systems and double excitations are beyond the capability of the present GW + BSE scheme; it is still challenging in treating strongly correlated systems containing *d*/*f* electrons; and so forth.

ACKNOWLEDGMENTS

Support by the National Natural Science Foundation of China (Grants Nos. 21173130, 21433006, and 21573131) is acknowledged.

REFERENCES

1. Feynman RP. Space-time approach to non-relativistic quantum mechanics. *Rev Mod Physics* 1948, 20:367–387.
2. Schwinger J. On the Green's functions of quantized fields: I. *Proc Natl Acad Sci USA* 1951, 37:452–455.
3. Onida G, Reining L, Rubio A. Electronic excitations: density-functional versus many-body Green's-function approaches. *Rev Mod Phys* 2002, 74:601–659.
4. Danovich D. Green's function methods for calculating ionization potentials, electron affinities, and excitation energies. *Wiley Interdiscip Rev Computat Mol Sci* 2011, 1:377–387.
5. Hedin L. New method for calculating the one-particle Green's function with application to electron-gas problem. *Phys Rev* 1965, 139:A796–A823.
6. Dyson FJ. The S matrix in quantum electrodynamics. *Phys Rev* 1949, 75:1736–1755.
7. Hybertsen MS, Louie SG. First-principles theory of quasiparticles: calculation of band gaps in semiconductors and insulators. *Phys Rev Lett* 1985, 55:1418–1421.
8. Salpeter EE, Bethe HA. A relativistic equation for bound-state problems. *Phys Rev* 1951, 84:1232–1242.
9. Sham LJ, Rice TM. Many-particle derivation of the effective-mass equation for the Wannier exciton. *Phys Rev* 1966, 144:708–714.
10. Hanke W, Sham LJ. Dielectric response in the Wannier representation: application to the optical spectrum of diamond. *Phys Rev Lett* 1974, 33:582–585.
11. Hanke W, Sham LJ. Many-particle effects in the optical excitations of a semiconductor. *Phys Rev Lett* 1979, 43:387–390.
12. Baym G, Kadanoff LP. Conservation laws and correlation functions. *Phys Rev* 1961, 124:287–299.
13. Strinati G. Dynamical shift and broadening of core excitons in semiconductors. *Phys Rev Lett* 1982, 49:1519–1522.
14. Onida G, Reining L, Godby RW, Sole RD, Andreoni W. Ab Initio calculations of the quasiparticle and absorption spectra of clusters: the sodium tetramer. *Phys Rev Lett* 1995, 75:818–821.
15. Hedin L, Lundqvist S. Effects of electron–electron and electron–phonon interactions on the one-electron states of solids. In: Seitz F, Turnbull D, Ehrenreich H, eds. *Solid State Physics, Advances in Research and Application*, vol. 23. New York: Academic Press; 1969, 1–181.
16. Hedin L. On correlation effects in electron spectroscopies and the GW approximation. *J Phys-Condens Matter* 1999, 11:R489–R528.
17. Strinati G. Application of the Green's functions method to the study of the optical properties of semiconductors. *Riv Nuovo Cimento* 1988, 11:1–86.
18. Aryasetiawan F, Gunnarsson O. The GW method. *Rep Prog Phys* 1998, 61:237–312.
19. Aulbur WG, Jonsson L, Wilkins JW. Quasiparticle calculations in solids. In: Ehrenreich H, Spaepen S, eds. *Solid State Physics, Advances in Research and Application*, vol. 54. New York: Academic Press; 2000, 1–218.
20. Ping Y, Rocca D, Galli G. Electronic excitations in light absorbers for photoelectrochemical energy conversion: first principles calculations based on many body perturbation theory. *Chem Soc Rev* 2013, 42:2437–2469.
21. Rinke P, Qteish A, Neugebauer J, Freysoldt C, Scheffler M. Combining GW calculations with exact-exchange density-functional theory: an analysis of valence-band photoemission for compound semiconductors. *New J Phys* 2005, 7:126.
22. Csanak GY, Taylor HS, Yaris R. Green's function technique in atomic and molecular physics. In: Bates DR, Esterman I, eds. *Advances in Atomic and Molecular Physics*, vol. 7. Amsterdam: Elsevier; 1971, 287–361.
23. Guzzo M, Lani G, Sottile F, Romaniello P, Gatti M, Kas JJ, Rehr JJ, Silly MG, Sirotti F, Reining L. Valence electron photoemission spectrum of semiconductors: ab initio description of multiple satellites. *Phys Rev Lett* 2011, 107:166401.

24. Zhou JS, Kas JJ, Sponza L, Reshetnyak I, Guzzo M, Giorgetti C, Gatti M, Sottile F, Rehr JJ, Reining L. Dynamical effects in electron spectroscopy. *J Chem Phys* 2015, 143:184109.
25. Lischner J, Vigil-Fowler D, Louie SG. Satellite structures in the spectral functions of the two-dimensional electron gas in semiconductor quantum wells: a GW plus cumulant study. *Phys Rev B* 2014, 89:125430.
26. Lischner J, Vigil-Fowler D, Louie SG. Physical origin of satellites in photoemission of doped graphene: an ab initio GW plus cumulant study. *Phys Rev Lett* 2013, 110:146801.
27. Kas JJ, Rehr JJ, Reining L. Cumulant expansion of the retarded one-electron Green function. *Phys Rev B* 2014, 90:085112.
28. Caruso F, Lambert H, Giustino F. Band structures of plasmonic polarons. *Phys Rev Lett* 2015, 114:146404.
29. Hybertsen MS, Louie SG. Electron correlation in semiconductors and insulators: band gaps and quasiparticle energies. *Phys Rev B* 1986, 34:5390–5413.
30. Godby RW, Needs RJ. Metal-insulator transition in Kohn-Sham theory and quasiparticle theory. *Phys Rev Lett* 1989, 62:1169–1172.
31. von der Linden W, Horsch P. Precise quasiparticle energies and Hartree-Fock bands of semiconductors and insulators. *Phys Rev B* 1988, 37:8351–8362.
32. Engel GE, Farid B. Generalized plasmon-pole model and plasmon band structures of crystals. *Phys Rev B* 1993, 47:15931–15934.
33. Lischner J, Sharifzadeh S, Deslippe J, Neaton JB, Louie SG. Effects of self-consistency and plasmon-pole models on G W calculations for closed-shell molecules. *Phys Rev B* 2014, 90:115130.
34. Stankovski M, Antonius G, Waroquiers D, Miglio A, Dixit H, Sankaran K, Giantomassi M, Gonze X, Côté M, Rignanese G-M. G_0W_0 band gap of ZnO: effects of plasmon-pole models. *Phys Rev B* 2011, 84:241201(R).
35. Kang W, Hybertsen MS. Quasiparticle and optical properties of rutile and anatase TiO_2. *Phys Rev B* 2010, 82:085203.
36. Larson P, Dvorak M, Wu ZG. Role of the plasmon-pole model in the GW approximation. *Phys Rev B* 2013, 88:125205.
37. Shishkin M, Kresse G. Implementation and performance of the frequency-dependent GW method within the PAW framework. *Phys Rev B* 2006, 74:035101.
38. Blase X, Attaccalite C, Olevano V. First-principles GW calculations for fullerenes, porphyrins, phtalocyanine, and other molecules of interest for organic photovoltaic applications. *Phys Rev B* 2011, 83:115103.
39. Rieger MM, Steinbeck L, White ID, Rojas HN, Godby RW. The GW space-time method for the self-energy of large systems. *Comput Phys Commun* 1999, 117:211–228.
40. Ren XG, Rinke P, Blum V, Wieferink J, Tkatchenko A, Sanfilippo A, Reuter K, Scheffler M. Resolution-of-identity approach to Hartree-Fock, hybrid density functionals, RPA, MP2 and GW with numeric atom-centered orbital basis functions. *New J Phys* 2012, 14:053020.
41. Caruso F, Rinke P, Ren XG, Rubio A, Scheffler M. Self-consistent GW: all-electron implementation with localized basis functions. *Phys Rev B* 2013, 88:075105.
42. Lebègue S, Arnaud B, Alouani M, Bloechl PE. Implementation of an all-electron GW approximation based on the projector augmented wave method without plasmon pole approximation: application to Si, SiC, AlAs, NaH, and KH. *Phys Rev B* 2003, 67:155208.
43. Giantomassi M, Stankovski M, Shaltaf R, Gruning M, Bruneval F, Rinke P, Rignanese GM. Electronic properties of interfaces and defects from many-body perturbation theory: recent developments and applications. *Phys Status Solidi B-Basic Solid State Phys* 2011, 248:275–289.
44. Strinati G. Effects of dynamical screening on resonances at inner-shell thresholds in semiconductors. *Phys Rev B* 1984, 29:5718–5726.
45. Rohlfing M, Louie SG. Electron–hole excitations and optical spectra from first principles. *Phys Rev B* 2000, 62:4927–4944.
46. Rohlfing M, Krüger P, Pollmann J. Quasiparticle band-structure calculations for C, Si, Ge, GaAs and SiC using Gaussian-orbital basis sets. *Phys Rev B* 1993, 48:17791–17805.
47. Rohlfing M, Krüger P, Pollmann J. Efficient scheme for GW quasiparticle band-structure calculations with applications to bulk Si and to the Si(001)-(2X1) surface. *Phys Rev B* 1995, 52:1905–1917.
48. Bruneval F. Ionization energy of atoms obtained from GW self-energy or from random phase approximation total energies. *J Chem Phys* 2012, 136:194107.
49. Setten MJ, Weigend F, Evers F. The GW-method for quantum chemistry applications: theory and implementation. *J Chem Theory Comput* 2013, 9:232–246.
50. Blum V, Gehrke R, Hanke F, Havu P, Havu V, Ren XG, Reuter K, Scheffler M. Ab initio molecular simulations with numeric atom-centered orbitals. *Comput Phys Commun* 2009, 180:2175–2196.
51. Gulans A, Kontur S, Meisenbichler C, Nabok D, Pavone P, Rigamonti S, Sagmeister S, Werner U. Draxl C exciting: a full-potential all-electron package implementing density-functional theory and many-body perturbation theory. *J Phys-Condens Matter* 2014, 26:363202.

52. Friedrich C, Blügel S, Schindlmayr A. Efficient implementation of the GW approximation within the all-electron FLAPW method. *Phys Rev B* 2010, 81:125102.
53. Kotani T, van Schilfgaarde M. Quasiparticle self-consistent GW method: a basis for the independent-particle approximation. *Phys Rev B* 2007, 76:165106.
54. Rostgaard C, Jacobsen KW, Thygesen KS. Fully self-consistent GW calculations for molecules. *Phys Rev B* 2010, 81:085103.
55. Hirose D, Noguchi Y, Sugino O. All-electron GW plus Bethe–Salpeter calculations on small molecules. *Phys Rev B* 2015, 91:205111.
56. Olovsson W, Tanaka I, Mizoguchi T, Puschnig P, Ambrosch-Draxl C. All-electron Bethe–Salpeter calculations for shallow-core x-ray absorption near-edge structures. *Phys Rev B* 2009, 79:041102(R).
57. Vinson J, Rehr JJ, Kas JJ, Shirley EL. Bethe–Salpeter equation calculations of core excitation spectra. *Phys Rev B* 2011, 83:115106.
58. Deslippe J, Samsonidze G, Strubbe DA, Jain M, Cohen ML, Louie SG, Berkeley GW. A massively parallel computer package for the calculation of the quasiparticle and optical properties of materials and nanostructures. *Comput Phys Commun* 2012, 183:1269–1289.
59. Gonze X, Amadon B, Anglade PM, Beuken JM, Bottin F, Boulanger P, Bruneval F, Caliste D, Caracas R, Cote M, et al. ABINIT: first-principles approach to material and nanosystem properties. *Comput Phys Commun* 2009, 180:2582–2615.
60. Marini A, Hogan C, Grüning M, Varsano D. yambo: an ab initio tool for excited state calculations. *Comput Phys Commun* 2009, 180:1392–1403.
61. Govoni M, Galli G. Large scale GW calculations. *J Chem Theory Comput* 2015, 11:2680–2696.
62. Kresse G, Furthmüller J. Efficient iterative schemes for ab initio total-energy calculations using a plane-wave basis set. *Phys Rev B* 1996, 54:11169–11186.
63. Faber C, Duchemin I, Deutsch T, Blase X. Many-body Green's function study of coumarins for dye-sensitized solar cells. *Phys Rev B* 2012, 86:155315.
64. Martin-Samos L, Bussi G. SaX: an open source package for electronic-structure and optical-properties calculations in the GW approximation. *Comput Phys Commun* 2009, 180:1416–1425.
65. Koval P, Foerster D, Sánchez-Portal D. Fully self-consistent GW and quasiparticle self-consistent GW for molecules. *Phys Rev B* 2014, 89:155417.
66. Caruso F, Rinke P, Ren X, Scheffler M, Rubio A. Unified description of ground and excited states of finite systems: the self-consistent GW approach. *Phys Rev B* 2012, 86:081102(R).
67. Ku W, Eguiluz AG. Band-gap problem in semiconductors revisited: effects of core states and many-body self-consistency. *Phys Rev Lett* 2002, 89:126401.
68. Kutepov A, Savrasov SY, Kotliar G. Ground-state properties of simple elements from GW calculations. *Phys Rev B* 2009, 80:041103(R).
69. Shishkin M, Kresse G. Self-consistent GW calculations for semiconductors and insulators. *Phys Rev B* 2007, 75:235102.
70. Jiang H. The GW method: basic principles, latest developments and its applications for d- and f-electron systems. *Acta Phys-Chim Sin* 2010, 26:1017–1033.
71. van Schilfgaarde M, Kotani T, Faleev S. Quasiparticle self-consistent GW theory. *Phys Rev Lett* 2006, 96:226402.
72. Chantis AN, van Schilfgaarde M, Kotani T. Ab initio prediction of conduction band spin splitting in zinc blende semiconductors. *Phys Rev Lett* 2006, 96:086405.
73. Shishkin M, Marsman M, Kresse G. Accurate quasiparticle spectra from self-consistent GW calculations with vertex corrections. *Phys Rev Lett* 2007, 99:246403.
74. Bruneval F, Vast N, Reining L. Effect of self-consistency on quasiparticles in solids. *Phys Rev B* 2006, 74:045102.
75. Botti S, Marques MAL. Strong renormalization of the electronic band gap due to lattice polarization in the GW formalism. *Phys Rev Lett* 2013, 110:226404.
76. Shih BC, Xue Y, Zhang PH, Cohen ML, Louie SG. Quasiparticle band gap of ZnO: high accuracy from the conventional G_0W_0 approach. *Phys Rev Lett* 2010, 105:146401.
77. Friedrich C, Müller MC, Blügel S. Band convergence and linearization error correction of all-electron GW calculations: the extreme case of zinc oxide. *Phys Rev B* 2011, 83:081101(R).
78. Berger JA, Reining L, Sottile F. Efficient GW calculations for SnO_2, ZnO, and rubrene: the effective-energy technique. *Phys Rev B* 2012, 85:085126.
79. Samsonidze G, Jain M, Deslippe J, Cohen ML, Louie SG. Simple approximate physical orbitals for GW quasiparticle calculations. *Phys Rev Lett* 2011, 107:186404.
80. Tamblyn I, Darancet P, Quek SY, Bonev SA, Neaton JB. Electronic energy level alignment at metal-molecule interfaces with a GW approach. *Phys Rev B* 2011, 84:201402(R).
81. Berger JA, Reining L, Sottile F. Ab initio calculations of electronic excitations: collapsing spectral sums. *Phys Rev B* 2010, 82:041103(R).
82. Reining L, Onida G, Godby RW. Elimination of unoccupied-state summations in ab initio self-energy calculations for large supercells. *Phys Rev B* 1997, 56:R4301–R4304.

83. Giustino F, Cohen ML, Louie SG. GW method with the self-consistent Sternheimer equation. *Phys Rev B* 2010, 81:115105.
84. Lambert H, Giustino F. Ab initio Sternheimer-GW method for quasiparticle calculations using plane waves. *Phys Rev B* 2013, 88:075117.
85. Janssen JL, Rousseau B, Cote M. Efficient dielectric matrix calculations using the Lanczos algorithm for fast many-body G_0W_0 implementations. *Phys Rev B* 2015, 91:125120.
86. Wilson HF, Gygi F, Galli GL. Efficient iterative method for calculations of dielectric matrices. *Phys Rev B* 2008, 78:113303.
87. Wilson HF, Lu DY, Gygi F, Galli G. Iterative calculations of dielectric eigenvalue spectra. *Phys Rev B* 2009, 79:245106.
88. Pham TA, Nguyen HV, Rocca D, Galli G. GW calculations using the spectral decomposition of the dielectric matrix: verification, validation, and comparison of methods. *Phys Rev B* 2013, 87:155148.
89. Nguyen HV, Pham TA, Rocca D, Galli G. Improving accuracy and efficiency of calculations of photoemission spectra within the many-body perturbation theory. *Phys Rev B* 2012, 85:081101(R).
90. Rocca D, Gebauer R, Saad Y, Baroni S. Turbo charging time-dependent density-functional theory with Lanczos chains. *J Chem Phys* 2008, 128:154105.
91. Rojas HN, Godby RW, Needs RJ. Space-time method for ab initio calculations of self-energies and dielectric response functions of solids. *Phys Rev Lett* 1995, 74:1827–1830.
92. Umari P, Stenuit G, Baroni S. Optimal representation of the polarization propagator for large-scale GW calculations. *Phys Rev B* 2009, 79:201104(R).
93. Umari P, Stenuit G, Baroni S. GW quasiparticle spectra from occupied states only. *Phys Rev B* 2010, 81:115104.
94. Rohlfing M. Electronic excitations from a perturbative LDA plus GdW approach. *Phys Rev B* 2010, 82:205127.
95. Neuhauser D, Gao Y, Arntsen C, Karshenas C, Rabani E, Baer R. Breaking the theoretical scaling limit for predicting quasiparticle energies: the stochastic GW approach. *Phys Rev Lett* 2014, 113:076402.
96. Qiu DY, da Jornada FH, Louie SG. Optical spectrum of MoS_2: many-body effects and diversity of exciton states. *Phys Rev Lett* 2013, 111:216805.
97. Marom N, Ren XG, Moussa JE, Chelikowsky JR, Kronik L. Electronic structure of copper phthalocyanine from G_0W_0calculations. *Phys Rev B* 2011, 84:195143.
98. Sander T, Maggio E, Kresse G. Beyond the Tamm-Dancoff approximation for extended systems using exact diagonalization. *Phys Rev B* 2015, 92:045209.
99. Grüning M, Marini A, Gonze X. Exciton-plasmon states in nanoscale materials: breakdown of the Tamm-Dancoff approximation. *Nano Lett* 2009, 9:2820–2824.
100. Ma YC, Rohlfing M, Molteni C. Excited states of biological chromophores studied using many-body perturbation theory: effects of resonant-antiresonant coupling and dynamical screening. *Phys Rev B* 2009, 80:241405(R).
101. Ma YC, Rohlfing M, Molteni C. Modeling the excited states of biological chromophores within many-body Green's function theory. *J Chem Theory Comput* 2010, 6:257–265.
102. Leng X, Yin HB, Liang DM, Ma YC. Excitons and Davydov splitting in sexithiophene from first-principles many-body Green's function theory. *J Chem Phys* 2015, 143:114501.
103. Baumeier B, Andrienko D, Ma YC, Rohlfing M. Excited states of dicyanovinyl-substituted oligothiophenes from many-body Green's functions theory. *J Chem Theory Comput* 2012, 8:997–1002.
104. Baumeier B, Andrienko D, Rohlfing M. Frenkel and charge-transfer excitations in donor-acceptor complexes from many-body Green's functions theory. *J Chem Theory Comput* 2012, 8:2790–2795.
105. Yin HB, Ma YC, Mu JL, Liu CB, Rohlfing M. Charge-transfer excited states in aqueous DNA: insights from many-body Green's function theory. *Phys Rev Lett* 2014, 112:228301.
106. Duchemin I, Deutsch T, Blase X. Short-range to long-range charge-transfer excitations in the zincbacteriochlorin-bacteriochlorin complex: a Bethe–Salpeter study. *Phys Rev Lett* 2012, 109:167801.
107. Duchemin I, Blase X. Resonant hot charge-transfer excitations in fullerene-porphyrin complexes: many-body Bethe–Salpeter study. *Phys Rev B* 2013, 87:245412.
108. Boulanger P, Jacquemin D, Duchemin I, Blase X. Fast and accurate electronic excitations in cyanines with the many-body Bethe–Salpeter approach. *J Chem Theory Comput* 2014, 10:1212–1218.
109. Varsano D, Coccia E, Pulci O, Conte AM, Guidoni L. Ground state structures and electronic excitations of biological chromophores at Quantum Monte Carlo/Many Body Green's Function Theory level. *Comput Theor Chem* 2014, 1040–1041:338–346.
110. Conte AM, Guidoni L, Del Sole R, Pulci O. Many-body study of the photoisomerization of the minimal model of the retinal protonated Schiff base. *Chem Phys Lett* 2011, 515:290–295.
111. Faber C, Boulanger P, Duchemin I, Attaccalite C, Blase X. Many-body Green's function GW and Bethe–Salpeter study of the optical excitations in a paradigmatic model dipeptide. *J Chem Phys* 2013, 139:194308.

112. Jesser A, Rohrmüller M, Schmidt WG, Herres-Pawlis S. Geometrical and optical benchmarking of copper guanidine–quinoline complexes: insights from TD-DFT and many-body perturbation theory. *J Comput Chem* 2014, 35:1–17.
113. Rohrmüller M, Herres-Pawlis S, Witte M, Schmidt WG. Bis-μ-Oxo and μ-η^2:η^2-peroxo dicopper complexes studied within (time-dependent) density-functional and many-body perturbation theory. *J Comput Chem* 2013, 34:1035–1045.
114. Marini A, Del Sole R. Dynamical excitonic effects in metals and semiconductors. *Phys Rev Lett* 2003, 91:176402.
115. Furche F, Ahlrichs R. Adiabatic time-dependent density functional methods for excited state properties. *J Chem Phys* 2002, 117:7433–7447.
116. Liu J, Liang WZ. Molecular-orbital-free algorithm for the excited-state force in time-dependent density functional theory. *J Chem Phys* 2011, 134:044114.
117. Ismail-Beigi S, Louie SG. Excited-state forces within a first-principles Green's function formalism. *Phys Rev Lett* 2003, 90:076401.
118. Ismail-Beigi S, Louie SG. Self-trapped excitons in silicon dioxide: mechanism and properties. *Phys Rev Lett* 2005, 95:156401.
119. Conte AM, Ippoliti E, Del Sole R, Carloni P, Pulci O. Many-body perturbation theory extended to the Quantum Mechanics/Molecular Mechanics approach: application to indole in water solution. *J Chem Theory Comput* 2009, 5:1822–1828.
120. Kaczmarski MS, Ma YC, Rohlfing M. Diabatic states of a photoexcited retinal chromophore from ab initio many-body perturbation theory. *Phys Rev B* 2010, 81:115433.
121. Lischner J, Deslippe J, Jain M, Louie SG. First-principles calculations of quasiparticle excitations of open-shell condensed matter systems. *Phys Rev Lett* 2012, 109:036406.
122. Aryasetiawan F, Biermann S. Generalized Hedin's equations for quantum many-body systems with spin-dependent interactions. *Phys Rev Lett* 2008, 100:116402.
123. Sakuma R, Friedrich C, Miyake T, Blügel S, Aryasetiawan F. GW calculations including spin-orbit coupling: application to Hg chalcogenides. *Phys Rev B* 2011, 84:085144.
124. Aguilera I, Friedrich C, Blügel S. Spin-orbit coupling in quasiparticle studies of topological insulators. *Phys Rev B* 2013, 88:165136.
125. Ahmed T, Albers RC, Balatsky AV, Friedrich C, Zhu JX. GW quasiparticle calculations with spin-orbit coupling for the light actinides. *Phys Rev B* 2014, 89:035104.
126. Marini A. Ab initio finite-temperature excitons. *Phys Rev Lett* 2008, 101:106405.
127. Cannuccia E, Marini A. Effect of the quantum zero-point atomic motion on the optical and electronic properties of diamond and trans-polyacetylene. *Phys Rev Lett* 2011, 107:255501.
128. Giustino F, Yates JR, Souza I, Cohen ML, Louie SG. Electron–phonon interaction via electronic and lattice wannier functions: superconductivity in boron-doped diamond reexamined. *Phys Rev Lett* 2007, 98:047005.
129. Giustino F, Louie SG, Cohen ML. Electron–phonon renormalization of the direct band gap of diamond. *Phys Rev Lett* 2010, 105:265501.
130. Lazzeri M, Attaccalite C, Wirtz L, Mauri F. Impact of the electron–electron correlation on phonon dispersion: failure of LDA and GGA DFT functionals in graphene and graphite. *Phys Rev B* 2008, 78:081406(R).
131. Faber C, Janssen JL, Côté M, Runge E, Blase X. Electron–phonon coupling in the C-60 fullerene within the many-body GW approach. *Phys Rev B* 2011, 84:155104.
132. Yin ZP, Kutepov A, Kotliar G. Correlation-enhanced electron–phonon coupling: applications of GW and screened hybrid functional to bismuthates, chloronitrides, and other high-Tc superconductors. *Phys Rev X* 2013, 3:021011.
133. Antonius G, Ponce S, Boulanger P, Cote M, Gonze X. Many-body effects on the zero-point renormalization of the band structure. *Phys Rev Lett* 2014, 112:215501.
134. Faber C, Boulanger P, Attaccalite C, Cannuccia E, Duchemin I, Deutsch T, Blase X. Exploring approximations to the GW self-energy ionic gradients. *Phys Rev B* 2015, 91:155109.
135. Grossman JC, Rohlfing M, Mitas L, Louie SG, Cohen ML. High accuracy many-body calculational approaches for excitations in molecules. *Phys Rev Lett* 2001, 86:472–475.
136. Chiodo L, García-Lastra JM, Iacomino A, Ossicini S, Zhao J, Petek H, Rubio A. Self-energy and excitonic effects in the electronic and optical properties of TiO_2 crystalline phases. *Phys Rev B* 2010, 82:045207.
137. Vidal J, Botti S, Olsson P, Guillemoles JF, Reining L. Strong interplay between structure and electronic properties in $CuIn(S,Se)_2$: a first-principles study. *Phys Rev Lett* 2010, 104:056401.
138. Brivio F, Butler KT, Walsh A, van Schilfgaarde M. Relativistic quasiparticle self-consistent electronic structure of hybrid halide perovskite photovoltaic absorbers. *Phys Rev B* 2014, 89:155204.
139. Filip MR, Giustino F. GW quasiparticle band gap of the hybrid organic–inorganic perovskite $CH_3NH_3PbI_3$: effect of spin-orbit interaction, semicore electrons, and self-consistency. *Phys Rev B* 2014, 90:245145.

140. Hahn PH, Schmidt WG, Seino K, Preuss M, Bechstedt F, Bernholc J. Optical absorption of water: coulomb effects versus hydrogen bonding. *Phys Rev Lett* 2005, 94:037404.
141. Pham TA, Zhang C, Schwegler E, Galli G. Probing the electronic structure of liquid water with many-body perturbation theory. *Phys Rev B* 2014, 89:060202.
142. Swartz CW, Wu XF. Ab initio studies of ionization potentials of hydrated hydroxide and hydronium. *Phys Rev Lett* 2013, 111:087801.
143. Kong LZ, Wu XF, Car R. Roles of quantum nuclei and inhomogeneous screening in the x-ray absorption spectra of water and ice. *Phys Rev B* 2012, 86:134203.
144. Wang NP, Rohlfing M, Kruger P, Pollmann J. Fast initial decay of molecular excitations at insulator surfaces. *Phys Rev Lett* 2004, 92:216805.
145. Neaton JB, Hybertsen MS, Louie SG. Renormalization of molecular electronic levels at metal-molecule interfaces. *Phys Rev Lett* 2006, 97:216405.
146. Garcia-Lastra JM, Thygesen KS. Renormalization of optical excitations in molecules near a metal surface. *Phys Rev Lett* 2011, 106:187402.
147. Migani A, Mowbray DJ, Zhao J, Petek H. Quasiparticle interfacial level alignment of highly hybridized frontier levels: H_2O on TiO_2(110). *J Chem Theory Comput* 2014, 11:239–251.
148. Sun H, Mowbray DJ, Migani A, Zhao J, Petek H, Rubio A. Comparing quasiparticle H_2O level alignment on anatase and rutile TiO_2. *Acs Catalysis* 2015, 5:4242–4254.
149. Pham TA, Lee D, Schwegler E, Galli G. Interfacial effects on the band edges of functionalized Si surfaces in liquid water. *J Am Chem Soc* 2014, 136:17071–17077.
150. Kharche N, Muckerman JT, Hybertsen MS. First-principles approach to calculating energy level alignment at aqueous semiconductor interfaces. *Phys Rev Lett* 2014, 113:176802.
151. Patrick CE, Giustino F. Quantitative analysis of valence photoemission spectra and quasiparticle excitations at chromophore-semiconductor interfaces. *Phys Rev Lett* 2012, 109:116801.
152. Verdi C, Mosconi E, De Angelis F, Marsili M, Umari P. Alignment of energy levels in dye/semiconductor interfaces by GW calculations: effects due to coadsorption of solvent molecules. *Phys Rev B* 2014, 90:155410.
153. Caruso F, Filip MR, Giustino F. Excitons in one-dimensional Van der Waals materials: Sb_2S_3 nanoribbons. *Phys Rev B* 2015, 92:125134.
154. Choi JH, Cui P, Lan HP, Zhang ZY. Linear scaling of the exciton binding energy versus the band gap of two-dimensional materials. *Phys Rev Lett* 2015, 115:066403.
155. Mu JL, Ma YC, Yin HB, Liu CB, Rohlfing M. Photoluminescence of single-walled carbon nanotubes: the role of Stokes shift and impurity levels. *Phys Rev Lett* 2013, 111:137401.
156. Freysoldt C, Eggert P, Rinke P, Schindlmayr A, Scheffler M. Screening in two dimensions: GW calculations for surfaces and thin films using the repeated-slab approach. *Phys Rev B* 2008, 77:235428.
157. Spataru CD, Ismail-Beigi S, Benedict LX, Louie SG. Excitonic effects and optical spectra of single-walled carbon nanotubes. *Phys Rev Lett* 2004, 92:077402.
158. Rohlfing M. Redshift of excitons in carbon nanotubes caused by the environment polarizability. *Phys Rev Lett* 2012, 108:087402.
159. Mak KF, da Jornada FH, He KL, Deslippe J, Petrone N, Hone J, Shan J, Louie SG, Heinz TF. Tuning many-body interactions in graphene: the effects of doping on excitons and carrier lifetimes. *Phys Rev Lett* 2014, 112:207401.
160. Körbel S, Boulanger P, Duchemin I, Blase X, Marques MAL, Botti S. Benchmark many-body GW and Bethe–Salpeter calculations for small transition metal molecules. *J Chem Theory Comput* 2014, 10:3934–3943.
161. Jacquemin D, Duchemin I, Blase X. Benchmarking the Bethe–Salpeter formalism on a standard organic molecular set. *J Chem Theory Comput* 2015, 11:3290–3304.
162. van der Horst J-W, Bobbert PA, Michels MAJ, Brocks G, Kelly PJ. Ab initio calculation of the electronic and optical excitations in polythiophene: effects of intra- and interchain screening. *Phys Rev Lett* 1999, 83:4413–4416.
163. Hummer K, Ambrosch-Draxl C. Oligoacene exciton binding energies: their dependence on molecular size. *Phys Rev B* 2005, 71:081202(R).
164. Cudazzo P, Gatti M, Rubio A. Excitons in molecular crystals from first-principles many-body perturbation theory: picene versus pentacene. *Phys Rev B* 2012, 86:195307.
165. Sai N, Tiago ML, Chelikowsky JR, Reboredo FA. Optical spectra and exchange-correlation effects in molecular crystals. *Phys Rev B* 2008, 77:161306(R).
166. Sharifzadeh S, Biller A, Kronik L, Neaton JB. Quasiparticle and optical spectroscopy of the organic semiconductors pentacene and PTCDA from first principles. *Phys Rev B* 2012, 85:125307.
167. Tiago ML, Rohlfing M, Louie SG. Bound excitons and optical properties of bulk trans-polyacetylene. *Phys Rev B* 2004, 70:193204.

